Online-Journals.org

iJOE International Journal of Online and Biomedical Engineering

iJOE | eISSN: 2626-8493 | Vol. 22 No. 1 (2026) | OPEN ACCESS

https://doi.org/10.3991/ijoe.v22i01.58971

PAPER

Evaluation of the Effect of Model Deviation in Air-to-Ground Signal Propagation on Cell Area of Coverage

Ashraf A. Tahat[1] (✉), **Talal A. Edwan**[2]

[1]Princess Sumaya University for Technology, Amman, Jordan

[2]University of Jordan, Amman, Jordan

tahat@psut.edu.jo

ABSTRACT

With the broadening capacity of the Internet-of-Things (IoT) framework, unmanned aerial vehicles (UAVs) are predicted to contribute to the enhancement of the variety of means of offered IoT services if they are equipped with wireless connectivity modules (e.g., LTE, 5G/6G cellular, LPWAN, WiFi, and satellite) for information exchange. Within this IoT scheme that employs wireless cellular networking, an UAV could constitute an aerial base station to act as the intermediate layer of the communication scheme and architecture. High-fidelity communications are necessary to ensure the superior functionality of this architecture. Therefore, accurate propagation modeling of the air-to-ground (A-to-G) UAV transmissions in an aerial base station cell is a prerequisite for designing and conducting an investigation of the performance of UAVs in various network topologies. We investigate the resulting deviations of a generic A-to-G path-loss (PL) propagation model from that of a custom-constructed (*Empirical*) A-to-G PL and shadowing model, which is based on environment and field measurements in conjunction with a specific frequency channel and network topology. To this end, analysis of performed computer simulations and numerical calculations corroborates our findings. Our conducted research for this *dense urban* environment setting reveals that a Gaussian (*Normal*) probability distribution function, when compared with our *Empirical* one, will overestimate the likelihood of received signal power to be equal to or larger than a desired threshold level by up to 9% in the vicinity of the border of an UAV cell, in addition to the associated percentage coverage area in both of the considered cell topologies. This could provide for a cost-effective, scalable, and accurate algorithm implementation for wireless operators' coverage estimation and planning.

KEYWORDS

unmanned aerial vehicles (UAV), base station, drone-cell, propagation model, air-to-ground (A-to-G), Gaussian, empirical CDF, shadowing log-normal, coverage area

1 INTRODUCTION

The rapid growth of unmanned aerial vehicles (UAVs) in recent years has led to their increasing integration into a wide range of civilian and commercial applications,

Tahat, A. A., Edwan, T. A. (2026). Evaluation of the Effect of Model Deviation in Air-to-Ground Signal Propagation on Cell Area of Coverage. *International Journal of Online and Biomedical Engineering (iJOE)*, 22(1), pp. 40–56. https://doi.org/10.3991/ijoe.v22i01.58971

Article submitted 2025-10-01. Revision uploaded 2025-11-01. Final acceptance 2025-11-03.

gradually becoming a mainstream technology. The global UAV market size is projected to grow from $41.26 billion in 2025 to $125.91 billion by 2032 [1]. According to the most recent data from the Federal Aviation Administration (FAA), 822,039 drones are registered in the United States as of July 2025. UAVs are deployed not only in military operations, but also in various civilian roles, including cargo delivery, weather monitoring, aerial photography and videography, intelligent transportation systems, public safety management, and emergency medical services, among others [2]–[6]. Many of these applications align with the broader concept of smart city services, and UAVs are even being considered for tasks such as Internet delivery.

With the continuous expansion of the Internet-of-Things (IoT) ecosystem [7], UAVs are expected to play a pivotal role in transforming the provision of IoT services [8], [9]. When equipped with wireless communication modules—such as cellular, Wi-Fi, wide-area networks (WAN), or satellite links—UAVs can facilitate cost-effective, value-added IoT services. Within cloud-enabled IoT frameworks, UAVs may function as edge devices, serving as an intermediate layer that bridges the sensors and the cloud infrastructure [9].

Given their increasing presence in both civilian and commercial domains, UAVs are also being explored as low-altitude aerial base stations or "drone-cells" to support future cellular networks [10]–[14]. As depicted in Figure 1, drone base stations offer rapid deployment capabilities to satisfy dynamic network demands, making the optimal placement of UAVs a critical challenge to maximize user coverage while maintaining a predefined quality of service (QoS) [12]–[14]. Although there is a growing body of research on UAV deployment as drone-cells, real-world implementations remain limited, and the identification of the most efficient network topologies is still an open research problem.

Reliable communication is fundamental for the safe operation and effective control of UAVs. Consequently, accurate modeling of the air-to-ground (A-to-G) propagation channel is essential for evaluating the performance of UAV communication systems and network topologies [15]–[17]. In the UAV context, A-to-G channels are broadly categorized into two classes: payload communications, which carry mission-related data such as video streams or sensor measurements, and control and non-payload communications (CNPC), which transmit telemetry and flight control commands critical for safe UAV operation. The characteristics of A-to-G channels—including path loss, fading, and line-of-sight (LoS) conditions—directly influence the quality and reliability of payload data [17]. In contrast, CNPC channels, although typically low in data rate, are highly critical, as any degradation or loss can compromise UAV safety or lead to mission failure. Therefore, CNPC channels are designed with stricter requirements for reliability, latency, and security.

Fig. 1. An UAV base station potential architecture

Most UAVs operate using generally available unlicensed frequency bands, with a significant portion of CNPC communications utilizing 2.4 GHz and 5.8 GHz. However, these spectrum bands are prone to congestion and are vulnerable to interference, making them less favorable from an aviation perspective. In the United States, CNPC communications are being considered for allocation in the L-band (0.9–1.2 GHz) and C-band (5.03–5.091 GHz), although regulatory usage of these bands remains under consideration [18], [19]. Importantly, A-to-G path-loss characteristics, to a large extent, are independent of the signaling purpose (payload or CNPC), aside from variations in carrier frequency and bandwidth. Historically, in the VHF range (118–137 MHz), amplitude modulation has been used for A-to-G communications since the 1940s.

Several studies have investigated A-to-G path-loss characteristics and developed associated models [20]–[28]. For instance, Matolak et al. conducted extensive measurement campaigns in the L-band (968 MHz) and C-band (5.06 GHz) for high-altitude UAV operations ranging from 500 to 2000 meters [20], [21]. In [23], the authors proposed an empirical model to estimate path loss and received signal strength (RSS) in outdoor urban scenarios across multiple frequency bands, including GSM (900 MHz), UMTS (1800 MHz), and LTE (2100 MHz) [29].

In this paper, however, we present an investigation of the resulting deviations of a generic A-to-G path-loss (PL) propagation model from that of a custom-constructed (*Empirical*) A-to-G PL and shadowing model, which is based on environment and field measurements in conjunction with a specific frequency channel and network topology. Our conducted research for this *dense urban* environment setting reveals that a Gaussian (*Normal*) probability distribution function, when compared with our *Empirical* one, will overestimate the likelihood of received signal power to be equal to or larger than a desired threshold level by up to 9% in the vicinity of the border of an UAV cell, in addition to the associated percentage coverage area in both of the considered cell topologies. This could provide for a cost-effective, scalable, and accurate algorithm implementation for wireless operators' coverage estimation and planning. The remainder of this paper is organized as follows: In Section 2, we present our review of the literature related to this work. Section 3, provides a presentation of the system model and fundamental theory. In Section 4, we perform an analysis of the field measurements data set to fit the A-to-G propagation model to the considered environment, accompanied by parameter extraction. We present our simulations and numerical results in Section 5. Finally, we draw conclusions in Section 6.

2 RELATED WORKS

Air-to-ground (A-to-G) propagation modeling for UAVs has been intensively studied due to the unique elevation-dependent characteristics of such links, which differ fundamentally from terrestrial channels. Extensive surveys—most notably the comprehensive review by Khawaja et al. [17] and C. Yan et al. [30] summarized empirical findings, modeling methodologies, and open research challenges. These works emphasize that accurate A-to-G modeling requires environment-specific parameterization and that elevation-angle–dependent LoS probability functions are essential to capture realistic link behavior.

Large-scale experimental campaigns by Matolak and Sun [20], [21] established a detailed measurement-based A-to-G channel models in the L- and C-bands across multiple environments, revealing close-to-free-space path loss under LoS conditions and strong Ricean fading statistics. Their results demonstrated that both path-loss exponents and shadowing factors depend strongly on altitude, terrain, and frequency—findings that directly motivate probabilistic and hybrid models such as the

elevation-angle-based formulation proposed by Al-Hourani et al. [25], [26]. The latter integrates LoS and NLoS excess-loss parameters with a sigmoidal LoS probability and remains a widely adopted analytic model for UAV coverage and placement studies.

At the standardization level, 3GPP TR 36.777 (2017) [31] formally documented channel-modeling guidelines for aerial users in LTE networks, identifying increased base-station visibility, interference coupling, and altitude-dependent link statistics as critical factors. Subsequent 3GPP studies on New-Radio aerial support [32] reinforced the necessity of environment-validated A-to-G models for interference analysis and performance evaluation of UAV-enabled cellular networks.

More recent surveys and measurement campaigns have further refined the understanding of UAV channels. The survey by Mao et al. [15] categorizes channel-sounding platforms, measurement methodologies, and processing techniques, highlighting persistent challenges such as synchronization, antenna calibration, and environmental repeatability. Complementary overviews on channel non-stationarity [16] and low-altitude communication integration [6] have drawn attention to the temporal and spatial variability of A-to-G links, particularly in dense urban environments.

Parallel to empirical modeling, data-driven and deterministic approaches have gained traction. Studies such as Tahat et al. [27] applied machine-learning-based regression and neural techniques to predict path loss in urban conditions. At the same time, hybrid ray-tracing-plus-statistical models exploit building-geometry information to improve spatial prediction accuracy [33], [34]. Although these techniques can outperform traditional analytical models, their applicability is limited by the requirement for large, site-specific datasets or detailed 3-D environmental maps.

A recurring assumption throughout most A-to-G modeling literature is the use of a log-normal (*Gaussian* in dB) shadowing model, typically combined with a log-distance path-loss expression (e.g., Eq. (5) shown later in this paper). However, comparative measurement analyses (e.g., [20], [21], [23], [24]) and recent statistical reviews (e.g., [17], [15]) report deviations from strict log-normality—often showing heavy-tailed or multimodal empirical error distributions that vary with altitude and environment. These deviations affect the accuracy of predicted coverage probabilities and system-level performance metrics.

Accordingly, several recent works advocate empirical or nonparametric approaches that use measurement-derived cumulative distribution functions (CDFs) instead of enforcing the Gaussian assumption [16], [34]. The present study directly aligns with this direction by constructing an environment-specific empirical CDF of shadowing at 5.8 GHz and comparing it to the Gaussian model (shown later in this paper in Figure 6), thereby quantifying the error introduced by assuming log-normality in UAV cell-coverage analysis. The results complement the foundational analytic models [25], [26] and measurement-based studies [20], [21], providing a refined perspective on realistic A-to-G channel behavior.

3 SYSTEM MODEL

3.1 UAV placement and spatial user distribution

A quasi-stationary UAV configured with a restricted transmission power will be launched to supplement or provide coverage for a crowded terrestrial cell with a defined coverage area, following the approach in [13] and [14]. To model the heterogeneous nature of user locals in different macrocell environments, they are assumed to be randomly and uniformly dispersed across the area of concern. Each user *i* has a

known location denoted by coordinates (x_i, y_i). The UAV's three-dimensional position is defined by its altitude h and its coordinates (x_D, y_D). An illustration of this model, assuming an ideal circular cell of radius R, is provided in Figure 2. In Figure 2, the dimension z corresponds to h, although it is shown as the depth dimension in the legend at the bottom right.

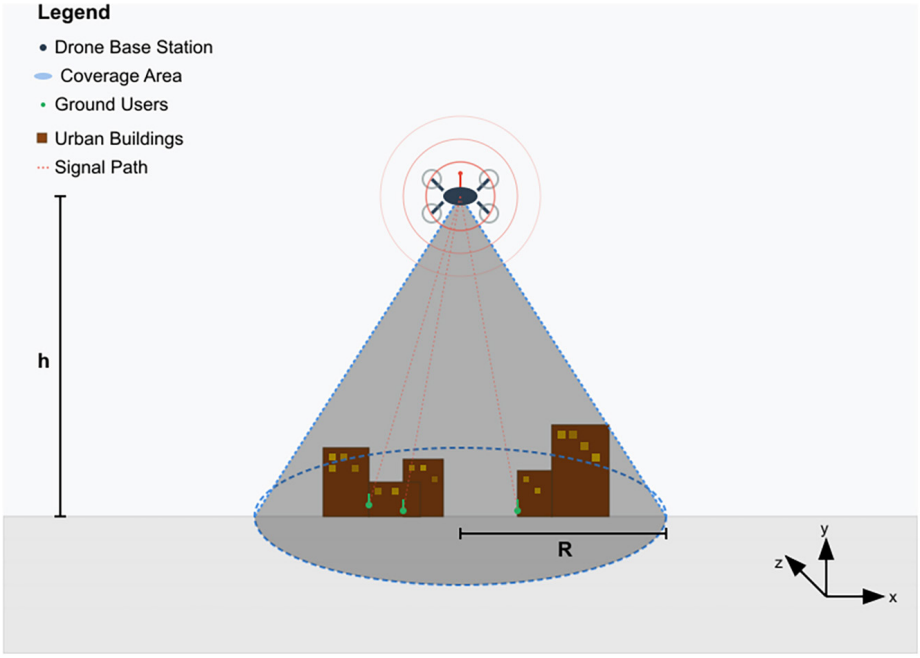

Fig. 2. An illustration of the coverage zone by an UAV base station structure

The selection of the UAV's 3D position, which establishes an auxiliary "aerial-cell," is critical as it determines each of the number of users the UAV can cover, and the A-to-G communication links quality. For a user to be considered within the coverage area and eligible for service, the observed signal-to-noise ratio (SNR)—a key indicator of quality of service (QoS) (or equivalently received signal power)—must exceed a predefined threshold. Consistent with [13] and [14], we assume a fixed QoS requirement for all terminals. Consequently, maximizing the served users' statistics equates to maximizing the revenue obtained from the service.

3.2 The A-to-G propagation model

In any communication link, received power and data rate are fundamental parameters for assessing quality and performance. A propagation model predicts the received power for each user, which in turn determines if the required QoS can be achieved. Since the link between the UAV aerial base station and each ground user is a wireless communication channel, an appropriate A-to-G channel model must be used. This work adopts the model from [14], which is identical to the one presented in [25], considering that the presence of a line-of-sight (LoS) connection is heavily influenced by the environment.

The likelihood of a LoS connection to the i^{th} user at location (x_i, y_i) is influenced by the altitude, h of UAV, and r_i, the horizontal distance from the center of the UAV-cell (x_D, y_D) to the position of this user. This distance is calculated as: $r_i = \sqrt{(x_D - x_i)^2 + (y_D - y_i)^2}$.

However, the probability of *LoS* is provided by [25] as:

$$P(h,r_i)=\frac{1}{1+a\exp\left(-b\left(\arctan\left(\frac{h}{r_i}\right)-a\right)\right)} \tag{1}$$

In (1), the constants a and b are selected based on the specific environment. While this model does not include shadowing effects, the average path loss can be computed probabilistically as:

$$L(h,r_i)=20\log\left(\frac{4\pi f_c}{c}\right)+20\log\left(\sqrt{(h^2+r_i^2)}\right)+P(h,r_i)\eta_{LoS}+\left(1-P(h,r_i)\right)\eta_{NLoS} \tag{2}$$

Here, f_c is the carrier frequency in Hz, and c is the speed of light in m/s. The terms η_{LoS} and η_{NLoS} represent the link losses (in dB) for *LoS* and non-line-of-sight (N_{LoS}) paths, respectively. We note that Eq. (2) may be simplified to:

$$L(h,r_i)=20\log\left(\sqrt{(h^2+r_i^2)}\right)+A\,P(h,r_i)+B \tag{3}$$

Where $A=\eta_{LoS}-\eta_{NLoS}$, and $B=20\log\left(\frac{4\pi f_c}{c}\right)+\eta_{NLoS}$. It is noted that (3) clearly shows that the path loss function depends on the vertical dimension h and the horizontal dimension r_i. For convenience, Tables 1 and 2 numerate the parameter values for different environments, as reported in [25] and [26].

Table 1. The S-Curve parameters for designated propagation environments

Environment Type	Parameters (a, b)
Suburban	(4.88, 0.43)
Urban	(9.61, 0.16)
Dense Urban	(12.08, 0.11)
High-rise Urban	(27.23, 0.08)

Table 2. Propagation losses (in dB) in designated environments at 5800 MHz

Environment Type	Parameters (η_{LoS}, η_{NLoS})
Suburban	(0.2, 24)
Urban	(1.2, 23)
Dense Urban	(1.8, 26)
High-rise Urban	(2.5, 41)

3.3 The log-distance path loss model

Analytical and empirical propagation models demonstrate that the average power of a received radio signal decays logarithmically with distance at a given frequency. This path loss can be modeled as [28], [36]:

$$\overline{PL}(d_i)=\overline{PL}(d_0)+10n\log\left(\frac{d_i}{d_0}\right) \tag{4}$$

In (4), n represents the path loss exponent. $PL(d_0)$ represents the path loss from the transmitter at a reference distance, d_0. The exponent n serves as an attenuation factor that incorporates the effects of all propagation mechanisms in the environment. Typically, n is greater than 2 (the free-space value) and can be as high as 5. In confined environments such as tunnels and building corridors, n can be less than 2.

A limitation of the standard log-distance model is that it does not account for differences in environmental clutter at different sites with the same transmitter-receiver separation distances. As a result, observed measured signal levels can deviate significantly from the predicted average. Measurements show that, at a specific distance d, the path loss $PL(d)$ is a random variable with a *log-normal* distribution (*normal* when expressed in dB) around the mean value. This leads to a more accurate model:

$$PL(d_i) = \overline{PL}(d_0) + 10n\log\left(\frac{d_i}{d_0}\right) + X_\sigma \tag{5}$$

Or, equivalently:

$$PL(d_i) = \overline{PL}(d_i) + X_\sigma \tag{6}$$

where, $\overline{PL}(d_i)$ represents the mean value of the path-loss computed at distance d_i, and X_σ is a zero-mean *Gaussian* random variable with standard deviation σ (in dB). Using linear regression, the values of n and σ can be derived from environment-measured data.

Since $PL(d)$ is a *normally* distributed random variable (in dB), the received power $P_r(d)$ is also *normally* distributed (in dB). The Q-function or error function (*erf*) can therefore be utilized to calculate the likelihood that the received signal level exceeds a specific threshold γ:

$$\mathbf{P}(P_r(d_i > \gamma)) = Q\left(\frac{\gamma - \overline{PL}(d_i)}{\sigma}\right) \tag{7}$$

$$\text{where } Q(z) = \frac{1}{\sqrt{2\pi}}\int_z^\infty exp\left(\frac{-x^2}{2}\right)dx \tag{8}$$

3.4 Determination of the percentage of coverage area

Within a coverage area, some locations will experience signal levels below a desired threshold due to random shadowing. It is useful to relate the probability of coverage at the cell boundary to the percentage of the total area that is covered. For a circular cell of radius R around a base station and a desired signal threshold γ (in dBm), we aim to compute $U(\gamma)$, the percentage of area where the received signal power is at or above γ, using a specified coverage probability at the cell boundary [29].

The separation distance between the UAV and the position of a user is:

$$d(h,r_i) = \sqrt{(h^2 + r_i^2)} \tag{9}$$

The path loss can be described in equation form by combining models as:

$$PL(d_i) = 20\log(d_i) + AP(h,r_i) + B + X_\sigma \tag{10}$$

The received power is then:

$$P_r(d_i) = P_T - PL(d_i) \tag{11}$$

Thus, the percentage of the useful service area is computed by integrating the coverage probability over the total area [29]:

$$U(\gamma) = \frac{1}{\pi R^2} \int_0^{2\pi} \int_0^R \mathbf{P}(P_r(r_i) > \gamma) r dr d\theta \tag{12}$$

In order to investigate the behavior of (12), we evaluate it for various h and the probability of the received power being larger than γ at the cell boundary R. The results are illustrated in Figure 3, where, $h = \{50, 100, 200\}$ meters, average $PL(d_0) =$ 40 dB, $d_0 = 1$ meter, $n = 3.5$ and $R = 500$ meters. Here, $d = R$.

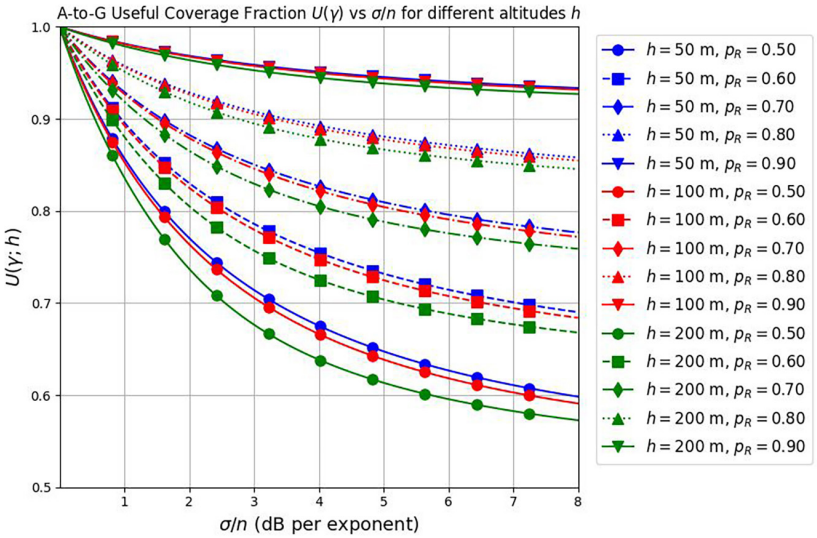

Fig. 3. Percentage of the useful service area for various UAV heights versus σ/n

4 ANALYSIS OF MEASUREMENT DATA AND ENVIRONMENT MODEL

4.1 Analysis of field measurements and fitting to the A-to-G propagation model

In our investigation, we generated a data set for our considered area of investigation within the vicinity of the PSUT campus to be superimposed on the existing and exact geographic locations extracted from the data set of the measurement campaign presented by the authors of [27] that contains 492 instances at each nominal frequency. In this work, we analyze and study the 5.8 GHz frequency band. The collected measurements from the high altitude flying platform (HAFP) (balloon) spanned a relative height, which increased from approximately 60 meters above the ground surface to a maximum height of roughly 1650 meters. The ground vehicle (GV) unit collecting the measurements scanned a designated path illustrated in Figure 4, which surrounds the original ground launch location of HAFP with an approximate horizontal radius of 1000 meters. The resulting path loss at the 5.8 GHz versus diagonal separation distance to the GV locations are plotted in Figure 5.

Fig. 4. Mobile terminal measurement locations from the HAFP [27]

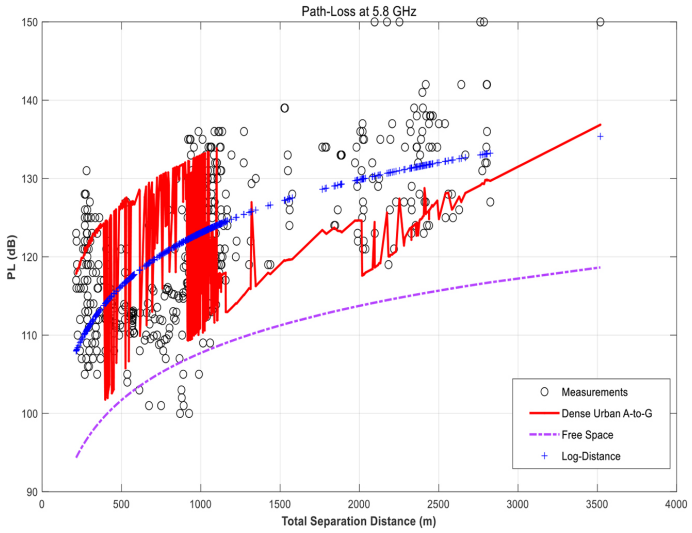

Fig. 5. Field measurements A-to-G PL at 5.8 GHz vs. distance and PL models

We generated our data set for this considered geographic area of investigation using the A-to-G model of (2) at 5.8 GHz in the four different environments listed in Section 3.2 (i.e., *suburban*, *urban*, *dense urban*, and *high-rise urban*):

$$L(h,r_i) = 20\log\left(\frac{4\pi f_c}{c}\right) + 20\log\left(\sqrt{(h^2 + r_i^2)}\right) + P(h,r_i)\eta_{LoS} + \left(1 - P(h,r_i)\right)\eta_{NLoS} \quad (13)$$

This geographic area resembles a *dense urban* environment in its building distribution and structure, in addition to surface clutter as depicted in Figure 4.

We then plotted the generated data set instances at the same GPS coordinates of the GV, including the relative altitude of the HAFP, superimposed on the original measurement data set points in Figure 5, to visually identify the correct environment classification by inspection, which indeed closely matches a *Dense Urban* environment as demonstrated by the plots of Figure 5.

For comparison purposes, we plotted the Log-Distance model of (14):

$$\overline{PL}(d_i) = \overline{PL}(d_0) + 10n\log\left(\frac{d_i}{d_0}\right) \tag{14}$$

By fitting it to the field measurements data set at 5.8 GHz as a function of the total diagonal separation distance between the HAFP and the receiver (GV), and using d_0 = 1 m. Model tuning and curve fitting algorithms in the Matlab® Curve Fitting Toolbox produced optimal parameters in (14), in the minimum mean-squared-error (MMSE) sense, for values of n = 1.98 and $\overline{PL}(d_0) = 63.45$. These values were used to plot the Log-Distance model curve as depicted in Figure 5.

4.2 Extraction of propagation model parameters from field measurements

The assumed A-to-G path loss model of (10) was used to extract the shadowing effect at each instance of the two data sets (difference between the field measurements and of generated A-to-G model values of (2), where the random variable, X_σ, in (10) represents the random fluctuations in the path loss values at a given distance, and deviation from the given mean value generated by the A-to-G model of (2) and (3). This process was performed for the four different environments listed in Section 3.2 (i.e., *suburban*, *urban*, *dense urban*, and *high-rise urban*).

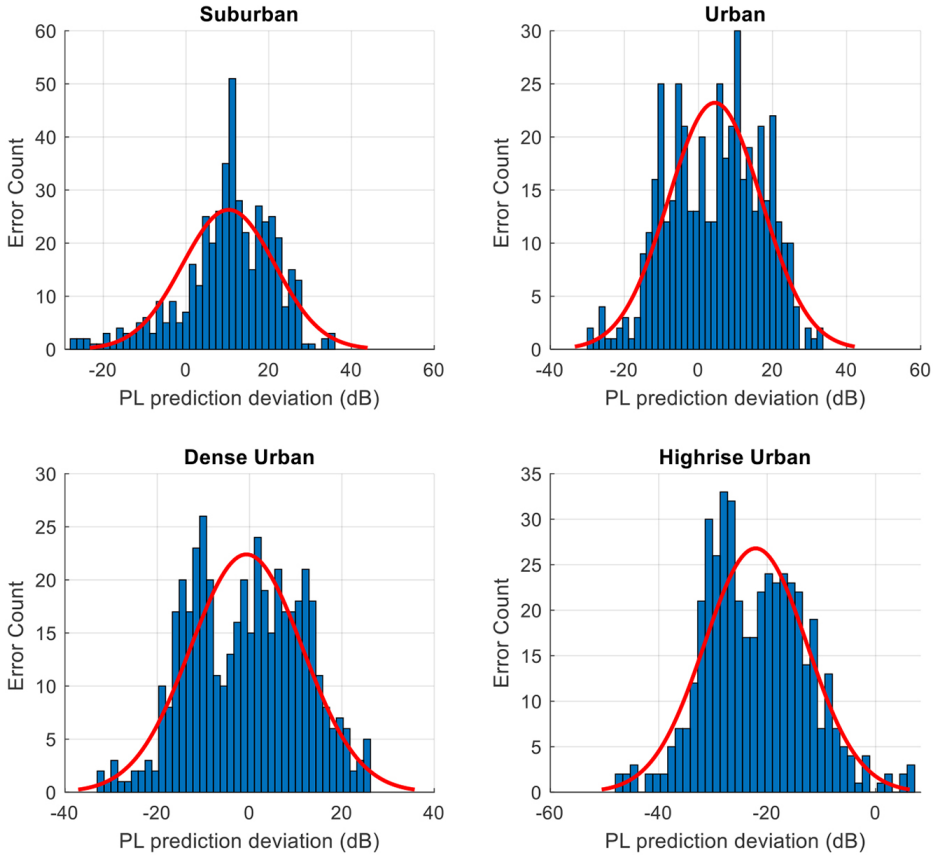

Fig. 6. Generated *Empirical* error histograms for 5.8 GHz center frequency data set and fitted *Normal* PDF for each environment category

The deviation in the predicted path loss values from the field measured values for all instances in the data set for the 5.8 GHz frequency was used to generate an *Empirical* error histogram for each environment category, as illustrated in Figure 6. We then fitted each of the *Empirical* error histograms with a Gaussian (*Normal*) probability distribution function (PDF) superimposed on the corresponding histogram subplot. Again, it is evident from these histograms and fitted plots that the *Dense Urban* environment category best matches the field measurement data set of the 5.8 GHz center frequency since it has the minimum *mean* of the four at –0.6713 dB, and a *standard deviation* of 12.1479 dB. We also generated an *Empirical* cumulative distribution function (CDF), as illustrated in Figure 7, for this environment category (i.e., the *dense urban*) calculated by the Kaplan-Meier estimate [35] using Matlab® to be utilized later in the numerical simulations and computational analysis and subsequent evaluation of the Cell Percentage of Coverage Area, U(γ) of (12).

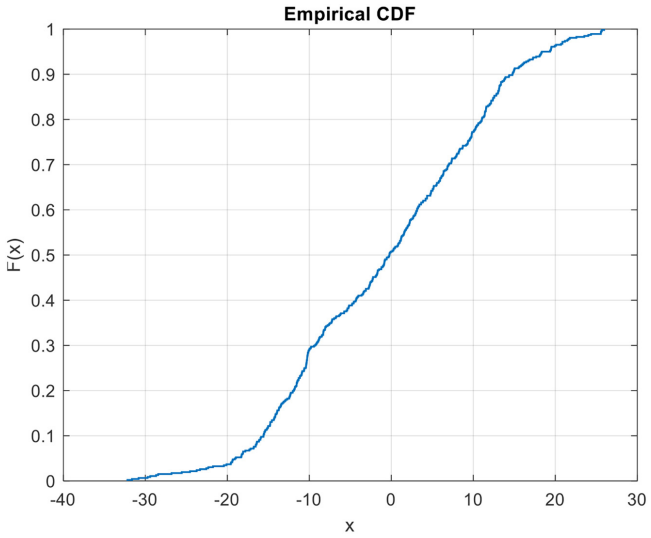

Fig. 7. An *Empirical* CDF extracted from data set for a *Dense Urban* A-to-G propagation model

5 SIMULATION AND NUMERICAL RESULTS

We consider two topologies of a wireless network cell coverage to analyze and compare the expected performance by calculating the percentage cell coverage for a defined position UAV auxiliary base station at a nominal height of h = 300 m. To this end, a Matlab® simulation was constructed, which considers a wireless network cell operating at a carrier frequency, f_c = 5.8 GHz. The cell topology represents a circular coverage footprint with borders having a maximum radius of R = 400 m for high data rate applications (e.g., LTE-U), and a cell radius of R = 1000 m for low data rate traffic (e.g., IoT terminals). It is assumed that the UAV-cell resources configuration will permit service in the region of coverage for all users associated with this serving base station. The served users in both topologies of the wireless network cell are assumed to be randomly uniformly distributed throughout the geographic cell coverage area as depicted in Figure 2.

The parameter values enumerated in Table 3 were utilized in evaluating the path loss in a hypothetical UAV-cell in the geographic area under consideration using (1) and (2) plotted in Figure 8, where it was identified to be of the *Dense Urban* environment category as was evident from the investigation and analysis conducted in Section 4.2. The horizontal distance varied from zero (i.e., cell center) to the

maximum of cell radius, R, in increments of 10 m. Path loss estimation at the same locations using the free-space propagation model was also plotted superimposed in Figure 8 as a reference benchmark.

Table 3. Simulation configuration parameters

Parametr	Value
Nominal frequency (f)	5800 MHz
Max. transmit power	40 dBm
Min received power (γ)	–80 dBm, –100 dBm
UAV height (h)	300 m
Cell radius (R)	400 m, 1000 m
Environment	*Dense Urban*

Since $P_r(d)$ and $PL(d)$ are random variables, we investigate the effect of deviation in using an assumed *Normal* (Gaussian) distribution CDF (with a mean and standard deviation as evaluated in Section 4.2) from using the generated environment specific *Empirical* CDF in conjunction with A-to-G propagation model of (2) to account for shadowing effects as in (8). Hence, we compute the probability that the received signal level is equal to or exceeds a target level γ (i.e., $\mathbf{P}(P_r(d_i \geq \gamma))$) at a border of the cell in a wireless cell topology associated with a particular application using (6) and using the CDF of Figure 7 as the true distribution in the environment under consideration. The numerical results are summarized in Table 4 for both of the two designated network topologies. In both cases, the *Normal* distribution assumption overestimates the likelihood of coverage at the cell boundary of receiving the desired power level. We also plotted $\mathbf{P}(P_r(d_i \geq \gamma))$ at different locations with varying distances from the center of the cell in Figures 9 and 10, for each of the network topologies (i.e., $R = 400$ m and $R = 1000$ m).

In addition, for each of the hypothetical circular coverage cell topologies, we computed the percentage of area, $U(\gamma)$, with a received signal level that is equal to or greater than $\gamma = -80$ dBm for high data rate traffic (e.g., LTE-U offloading), and equal to or greater than $\gamma = -100$ dBm for low data rate traffic (e.g., IoT terminals and sensors).

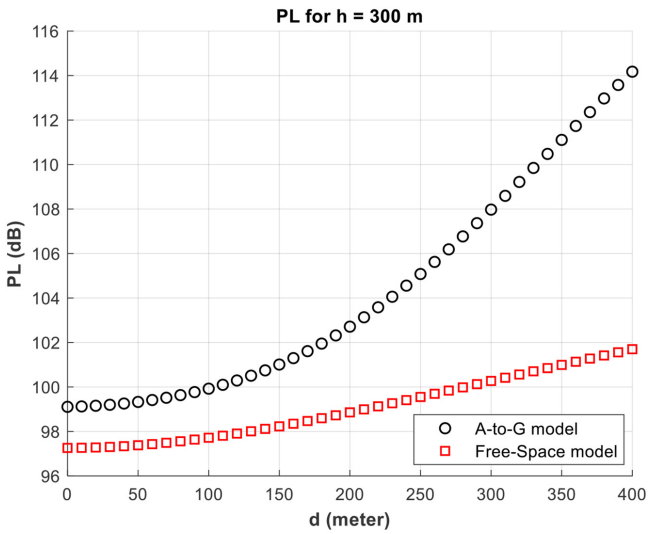

Fig. 8. Generated path loss in a hypothetical UAV cell in the geographic area under consideration

Table 4. Numerical results

Network Topology	P($P_r > \gamma$) at Cell Border with the *Empirical* CDF	P($P_r > \gamma$) at cell Border with the *Gaussian* CDF	Overestimate of P($P_r > \gamma$) in Percent	Uγ with the *Empirical* CDF	Uγ with the *Gaussian* CDF	Overestimate of Uγ in Percent
High data rate ($R = 400$ m)	0.6291	0.6644	*5.6%*	0.8125	0.8325	*2.5%*
Low data rate ($R = 1000$ m)r	0.6876	0.7494	*9.0%*	0.8524	0.8712	*2.2%*

Equation (12) was implemented in Matlab to compute U(γ), where the trapezoidal method of numerical integration was employed to approximate the integration operator. The resulting computed values of U(γ) are listed in Table 4 for both of the wireless network cell topologies.

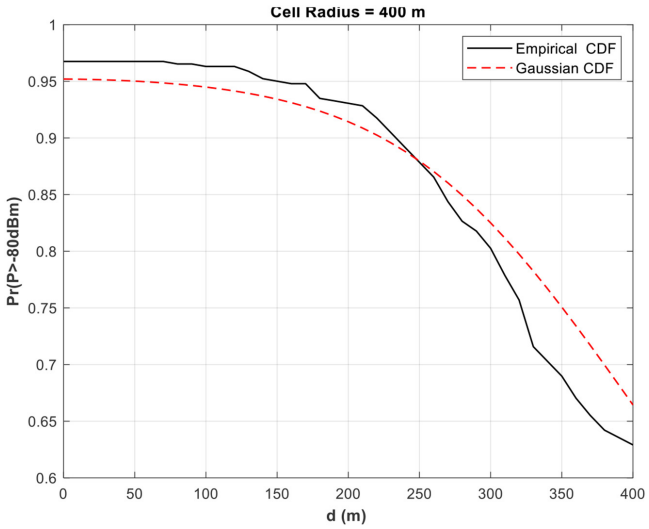

Fig. 9. Probability of received signal power P ≥ γ = –80 dBm with a high data rate network topology (LTE-U) with cell radius R = 400 m

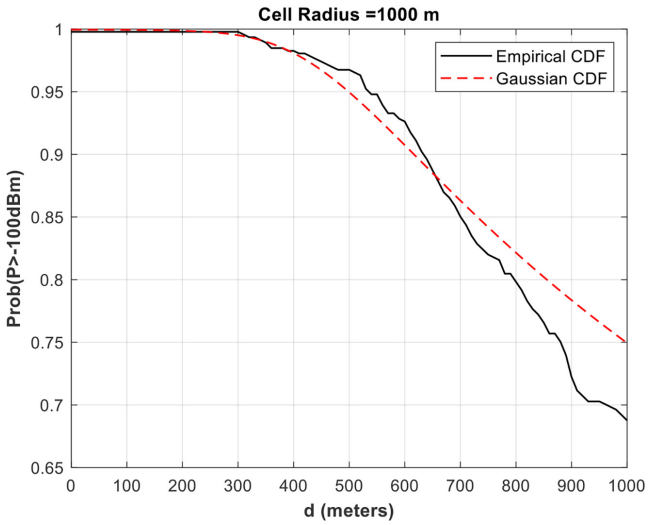

Fig. 10. Probability of received signal power P ≥ γ = –100 dBm with a low data rate network topology (IoT) with cell radius R = 1000 m

We compared the obtained U(γ) values based on the actual environment-derived *Empirical* CDF with those obtained relying on a *Gaussian* distribution with a mean and a standard deviation computed from the geographic area under consideration. Again, the *Gaussian* distribution overestimates the U(γ) in both of the network topologies.

6 CONCLUSIONS

Since accurate propagation modeling of the A-to-G UAV transmissions in an aerial base station cell is necessary for designing and conducting an analysis of the performance of UAVs in various network topologies, in this paper, we suggested and presented a methodology for constructing an accurate *Empirical* CDF to integrate environment-specific shadowing effects into A-to-G PL propagation model in an UAV base station. We investigated the resulting deviations of a generic A-to-G PL propagation model from that of our custom-constructed (*Empirical*) A-to-G PL and shadowing model, which was based on environment-specific field measurements in conjunction with a specific operating frequency and network topology. Analysis of performed computer simulations and numerical calculations confirmed our findings. Our conducted research for this *dense urban* environment setting reveals that a Gaussian (*Normal*) probability distribution function, when compared with our *Empirical* one, will overestimate the likelihood of received signal power to be equal to or larger than a desired threshold level by up to 9% in the vicinity of the border of an UAV cell, in addition to the associated percentage coverage area in both of the considered cell topologies. This could provide a cost-effective, scalable, and accurate algorithm for wireless operators' coverage estimation and planning.

6.1 Future works

Our focus in future research is to extend this investigation to include other frequency bands and to generalize the framework and methodology. Also, expanding its application to other types of PDFs for potential improvement in computational accuracy in the evaluation of the cell percentage of coverage area, U(γ) of (12). In addition, the proposed methodology and results need to be analyzed within other A-to-G PL models. Moreover, we will consider methodological approaches for extracting environment-specific shadowing effects in A-to-G PL models from satellite maps for this purpose.

7 ACKNOWLEDGEMENTS

This research and analysis were performed during a Sabbatical Leave of Prof. Ashraf Tahat from Princess Sumaya University for Technology (PSUT).

8 REFERENCES

[1] Fortune Business Insights, "Unmanned aerial vehicle market and trends," 2025. [Online]. Available: https://www.fortunebusinessinsights.com/industry-reports/unmanned-aerial-vehicle-uav-market-101603 [Accessed: Nov. 1, 2025].

[2] A. R. Ragab, P. F. Peña, M. A. Luna, and M. S. Ale Isaac, "Systemic integrated unmanned aerial system," *Int. Journal of Online Engineering*, vol. 18, no. 1, pp. 28–51, 2022. https://doi.org/10.3991/ijoe.v18i01.26435

[3] A. Hulaj, E. Bytyci, and V. Kadriu, "An efficient tasks scheduling algorithm for drone operations in the indoor environment," *Int. Journal of Online Engineering*, vol. 18, no. 11, pp. 42–57, 2022. https://doi.org/10.3991/ijoe.v18i11.29977

[4] J. Jiang, S. Gao, C. Li, Q. Zhang, and Q. Sun, "Improving the satellite-based winter wheat monitoring by using UAV-derived leaf chlorophyll content," *IEEE Journal of Selected Topics in Applied Earth Observations and Remote Sensing*, vol. 18, pp. 24242–24250, 2025. https://doi.org/10.1109/JSTARS.2025.3607431

[5] Y. Qin, M. A. Kishk, and M.-S. Alouini, "A survey on integrating UAVs into public safety networks: Advantages and potential risks," *IEEE Open Journal of the Communications Society*, vol. 6, pp. 9343–9372, 2025. https://doi.org/10.1109/OJCOMS.2025.3607987

[6] Y. Liu, X. Xie, Y. Kong, B. Zhang, and Y. Kang, "Survey on the integration of communication, sensing, and computing power for low-altitude UAVs," in *Proc. 7th International Conference on Electronics and Communication, Network and Computer Technology (ECNCT)*, 2025, pp. 196–207. https://doi.org/10.1109/ECNCT66493.2025.11172607

[7] F. Mahiri, A. Najoua, and S. Ben Souda, "5G-enabled IIoT framework architecture towards sustainable smart manufacturing," *Int. Journal of Online Engineering*, vol. 18, no. 4, pp. 4–20, 2022. https://doi.org/10.3991/ijoe.v18i04.27753

[8] Y. Zhang, Q. Wu, and J. Wang, "A wireless communication system of IoT based on UAV," in *Proc. 12th International Symposium on Parallel Architectures, Algorithms and Programming (PAAP)*, 2021, pp. 178–182. https://doi.org/10.1109/PAAP54281.2021.9720479

[9] A. Fotouhi *et al.*, "Survey on UAV cellular communications: Practical aspects, standardization advancements, regulation, and security challenges," *IEEE Communications Surveys & Tutorials*, vol. 21, no. 4, pp. 3417–3442, 2019. https://doi.org/10.1109/COMST.2019.2906228

[10] S.-C. Choi and S.-Y. Kim, "An independent UAV-based mobile base station," *Sensors*, vol. 25, no. 5, pp. 1–17, 2025. https://doi.org/10.3390/s25051349

[11] N. Sharma *et al.*, "Aerial base station assisted cellular communication: Performance and trade-off," *IEEE Transactions on Network Science and Engineering*, vol. 8, no. 4, pp. 2765–2779, 2021. https://doi.org/10.1109/TNSE.2021.3052984

[12] Z. Wang, S. X. Ng, and M. El-Hajjar, "A 3D spatial information compression-based deep reinforcement learning technique for UAV path planning in cluttered environments," *IEEE Open J. Veh. Technol.*, vol. 6, pp. 647–661, 2025. https://doi.org/10.1109/OJVT.2025.3540174

[13] A. Tahat *et al.*, "Optimal decision on placement of an auxiliary aerial wireless base station using the artificial bee colony algorithm," in *Proc. International Conference on Advanced Communication Technologies and Networking (CommNet)*, 2019, pp. 1–6. https://doi.org/10.1109/COMMNET.2019.8742386

[14] R. I. Bor-Yaliniz, A. El-Keyi, and H. Yanikomeroglu, "Efficient 3-D placement of an aerial base station in next generation cellular networks," in *Proc. IEEE International Conference on Communications (ICC)*, 2016, pp. 1–5. https://doi.org/10.1109/ICC.2016.7510820

[15] K. Mao *et al.*, "A survey on channel sounding technologies and measurements for UAV-assisted communications," *IEEE Transactions on Instrumentation and Measurement*, vol. 73, pp. 1–24, 2024. https://doi.org/10.1109/TIM.2024.3436128

[16] X. Cheng, Z. Huang, and L. Bai, "Channel nonstationarity and consistency or beyond 5G and 6G: A survey," *IEEE Communications Surveys & Tutorials*, vol. 24, no. 3, pp. 1634–1669, 2022. https://doi.org/10.1109/COMST.2022.3184049

[17] W. Khawaja *et al.*, "A survey of air-to-ground propagation channel modeling for unmanned aerial vehicles," *IEEE Communications Surveys Tutorials*, vol. 21, no. 3, pp. 2361–2391, 2019. https://doi.org/10.1109/COMST.2019.2915069

[18] B. Kerczewski, "Spectrum for UAS control and non-payload communications," in *Proc. IEEE Integr. Commun. Navig. Surveillance Conf. (ICNS)*, 2013, pp. 1–21. https://doi.org/10.1109/ICNSurv.2013.6548666

[19] B. R. Jackson, "Telemetry, command and control of UAS in the national airspace," in *Proc. Eur. Telemetry Test Conf.*, Nuremberg, Germany, 2016, pp. 145–155. https://doi.org/10.5162/etc2016/5.1

[20] D. W. Matolak and R. Sun, "Air-ground channels for UAS: Summary of measurements and models for L- and C-bands," in *Proc. Integrated Communications Navigation and Surveillance (ICNS)*, 2016, pp. 1–11. https://doi.org/10.1109/ICNSURV.2016.7486380

[21] D. W. Matolak and R. Sun, "Unmanned aircraft systems: Air-ground channel characterization for future applications," *IEEE Vehicular Technology Magazine*, vol. 10, pp. 79–85, 2015. https://doi.org/10.1109/MVT.2015.2411191

[22] K. Wang *et al.*, "Path loss measurement and modeling for low-altitude UAV access channels," in *Proc. IEEE 86th Vehicular Technology Conference (VTC-Fall)*, 2017, pp. 1–5. https://doi.org/10.1109/VTCFall.2017.8288385

[23] T. Tavares *et al.*, "Generalized LUI propagation model for UAVs communications using terrestrial cellular networks," in *Proc. IEEE 82nd Vehicular Technology Conference (VTC2015-Fall)*, 2015, pp. 1–6. https://doi.org/10.1109/VTCFall.2015.7390963

[24] A. Al-Hourani and K. Gomez, "Modeling cellular-to-UAV path-loss for suburban environments," *IEEE Wireless Communications Letters*, vol. 7, pp. 82–85, 2018. https://doi.org/10.1109/LWC.2017.2755643

[25] A. Al-Hourani, S. Kandeepan, and S. Lardner, "Optimal LAP altitude for maximum coverage," *IEEE Wireless Communications Letters*, vol. 3, no. 6, pp. 569–572, 2014. https://doi.org/10.1109/LWC.2014.2342736

[26] A. Al-Hourani, S. Kandeepan, and A. Jamalipour, "Modeling air-to-ground path loss for low altitude platforms in urban environments," in *Proc. IEEE Globecom*, 2014, pp. 2898–2984. https://doi.org/10.1109/GLOCOM.2014.7037248

[27] A. Tahat, T. Edwan, H. Al-Sawwaf, J. Al-Baw, and M. Amayreh, "Simplistic machine learning-based air-to-ground path loss modeling in an urban environment," in *Proc. Fifth International Conference on Fog and Mobile Edge Computing (FMEC)*, 2020, pp. 158–163. https://doi.org/10.1109/FMEC49853.2020.9144965

[28] A. Saakian, *Radio Wave Propagation Fundamentals*. Norwood, MA: Artech House, 2011.

[29] F. Richter, A. J. Fehske, and G. P. Fettweis, "Energy efficiency aspects of base station deployment strategies for cellular networks," in *Proc. IEEE 70th Vehicular Technology Conference Fall*, Anchorage, AK, USA, 2009, pp. 1–5. https://doi.org/10.1109/VETECF.2009.5379031

[30] C. Yan, L. Fu, J. Zhang, and J. Wang, "A comprehensive survey on UAV communication channel modeling," *IEEE Access*, vol. 7, pp. 107769–107792, 2019. https://doi.org/10.1109/ACCESS.2019.2933173

[31] 3GPP TR 36.777 V15.0.0, "Study on enhanced LTE support for aerial vehicles," 3rd Generation Partnership Project (3GPP), 2017.

[32] 3GPP TR 38.901 V17.0.0, "Study on channel model for frequencies from 0.5 to 100 GHz," 3rd Generation Partnership Project (3GPP), 2022.

[33] X. Yang, D. Zhai, R. Zhang, L. Liu, J. Du, and V. C. M. Leung, "A geometry-based stochastic channel model for UAV-to-ground integrated sensing and communication scenarios," *IEEE Trans. Veh. Technol.*, vol. 74, no. 4, pp. 5307–5320, 2025. https://doi.org/10.1109/TVT.2024.3510063

[34] H. Li *et al.*, "Air-to-ground path-loss prediction using ray-tracing and measurement-data jointly driven DNN," *Computer Communications*, vol. 196, pp. 268–276, 2022. https://doi.org/10.1016/j.comcom.2022.10.007

[35] J. F. Lawless, *Statistical Models and Methods for Lifetime Data*. Hoboken, NJ: Wiley-Interscience, 2002. https://doi.org/10.1002/9781118033005

[36] T. Rappaport, *Wireless Communications: Principles and Practice*, 2nd ed. Upper Saddle River, NJ, USA: Prentice Hall PTR.

9 AUTHORS

Ashraf A. Tahat is a Professor of Electrical and Computer Engineering (ECE) at King Abdullah II School of Engineering in the Department of Communications and IoT Engineering of Princess Sumaya University for Technology (PSUT). Dr Tahat earned his PhD degree in ECE from the Illinois Institute of Technology (Illinois Tech) in Chicago, IL, USA, where he also earned his BScEE, and MScEE degrees. Dr Tahat was also an Adjunct Professor with the Department of ECE of Illinois Tech post completing his doctoral studies. In 2024, he completed the Leaders in Innovation Fellowships (LIF) program by the Royal Academy of Engineering in London (UK). Dr Tahat has versatile and global experiences combining industry and academic posts in addition to providing truly international consultations. In 2024–2025, he was a Professor at the School of Engineering and Technology of the American University for the Middle East (AUM) in Kuwait. Dr Tahat conceptualized masterminded the IoT Engineering program at PSUT, and participated in establishing the department, where he was the Department Chairman (2010–2012). In addition, Dr Tahat was a Visiting Professor in the Dept. of ECE at McGill University in Montreal, Quebec, Canada (2012–2013), conducting research to develop novel algorithms in conjunction with software simulations to optimize performance and verification. Moreover, his Industry experience includes government-funded applied research projects, such as with Efficient Protection Inc., and with Octasic Inc. jointly with the École de Technologie Supérieure at (ÉTS) in Montreal, Quebec, Canada. Furthermore, Dr Tahat's professional work involved conducting R&D as a Senior Staff Engineer at 3Com Corporation in the USA. He was also an R&D Consultant at the Concept Center of Bell Labs (Nokia Networks). Dr Tahat is the inventor of a US Patent relating to 4G and 5G wireless communications systems standards and applications. Among his sevral awards, Dr Tahat received the Philadelphia Best Invention Award, and the Arab Pioneers and Innovators Award. Professor Tahat was the Vice-Chairman of the IEEE-Jordan Section (2018–2022). He is a senior Member of IEEE/Eta Kappa Nu and of Tau Beta Pi honor societies (E-mail: tahat@psut.edu.jo).

Talal A. Edwan received a BSc in Electronics Engineering with First Class Honours (distinguished excellent GPA) from Princess Sumaya University for Technology (PSUT) in 2002, an MSc in Network Systems Engineering with Distinction from the University of Plymouth (UK) in 2005, and a PhD in Computer Networks—with an early PhD thesis submission award—from Loughborough University (UK) in 2010. The primary work of Dr Edwan has been in the areas of computer system performance evaluation and engineering, network protocols, and network algorithms. From 2002 to 2004, he worked as a Telecommunication Networks Engineer at the Ministry of Information and Communications Technology in Jordan. Dr Talal served as an Assistant Professor in the Department of Computer Engineering at PSUT from 2014 to 2019, and as an Assistant Professor in the Department of Computer Engineering at Al-Ahliyya Amman University (AAU) from 2020 to 2022. He is currently an Assistant Professor in the Department of Computer Engineering at the University of Jordan. His research interests include: Computer Networks, Performance Evaluation and Engineering of Computer Systems and Networks, and Analytical Modeling of Computer Systems (E-mail: t.edwan@ju.edu.jo).